Environmental Science & Technology

pubs.acs.org/est

Article

Particle Size Distribution Dynamics Can Help Constrain the Phase State of Secondary Organic Aerosol

Yicong He, Ali Akherati, Theodora Nah, Nga L. Ng, Lauren A. Garofalo, Delphine K. Farmer, Manabu Shiraiwa, Rahul A. Zaveri, Christopher D. Cappa, Jeffrey R. Pierce, and Shantanu H. Jathar*

Cite This: https://dx.doi.org/10.1021/acs.est.0c05796

Read Online

ACCESS | Metrics & More | Article Recommendations | Supporting Information

ABSTRACT: Particle phase state is a property of atmospheric aerosols that has important implications for the formation, evolution, and gas/particle partitioning of secondary organic aerosol (SOA). In this work, we use a size-resolved chemistry and microphysics model (Statistical Oxidation Model coupled to the TwO Moment Aerosol Sectional (SOM-TOMAS)), updated to include an explicit treatment of particle phase state, to constrain the bulk diffusion coefficient (D_b) of SOA produced from α-pinene ozonolysis. By leveraging data from laboratory experiments performed in the absence of a seed and under dry conditions, we find that the D_b for SOA can be constrained ($(1-7) \times 10^{-15}$ cm^2 s^{-1} in these experiments) by simultaneously reproducing the time-varying SOA mass concentrations and the evolution of the particle size distribution. Another version of our model that used the predicted SOA composition to calculate the glass-transition temperature, viscosity, and, ultimately, D_b ($\sim 10^{-15}$ cm^2 s^{-1}) of the SOA was able to reproduce the mass and size distribution measurements when we included oligomer formation (oligomers accounted for about a fifth of the SOA mass). Our work highlights the potential of a size-resolved SOA model to constrain the particle phase state of SOA using historical measurements of the evolution of the particle size distribution.

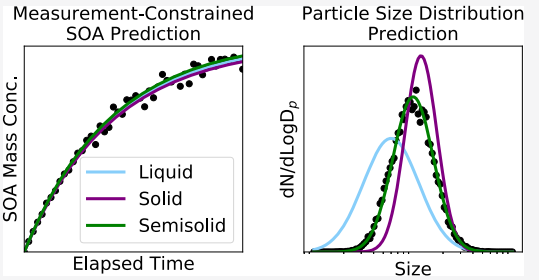

1. INTRODUCTION

Secondary organic aerosol (SOA) accounts for a substantial fraction of the submicron atmospheric aerosol burden and, consequently, has impacts on climate, air quality, and human health.[1,2] The particle phase state is an important property that likely affects the abundance and properties of atmospheric SOA since it has been shown to exert control on the equilibration timescale,[3] multiphase chemistry,[4,62] long-range transport of organic pollutants,[5,6,62] and formation of ice clouds.[7−9,62] However, there are large uncertainties in quantifying the evolving phase state of SOA and this has made it challenging to accurately represent the SOA phase state and its impacts in atmospheric models.

Anthropogenic and biogenic SOA formed from the oxidation of volatile organic compounds (VOCs) can be semisolid or viscous under a wide range of atmospheric conditions (0 < RH < 90% and T < 298 K).[10] As a model system, the SOA formed from the oxidation of α-pinene has been extensively probed to study its phase state.[11−18] The particle phase state is often quantified using the dynamic viscosity (ν; Pa·s) or the bulk diffusion coefficient (D_b; cm^2 s^{-1}); they are related to each other via the Stokes−Einstein equation ($D_b = \frac{kT}{6\pi a \nu}$, where k is the Boltzmann constant, T is the temperature, and a is the effective molecular diameter). The consensus seems to be that α-pinene-derived SOA is unlikely to behave like a liquid when formed and sampled under relatively dry conditions (RH < 30%) but the estimated phase state range for this SOA spans over 6 orders of magnitude; $\nu = 10^6-10^{12}$ Pa·s or $D_b = 10^{-15}-10^{-21}$ cm^2 s^{-1}.[11,13,14,16,18−20] Some of the uncertainty in the estimated particle phase state can be attributed to differences in the techniques used to probe the SOA. For instance, some have collected the SOA onto a media (e.g., filters, microscopy grids) and examined the flow properties of raw or reconstituted particles to estimate the viscosity.[13,16] Others have inferred viscosity of suspended particles by studying the bounce fraction on impaction plates[12,15] and the time for particles to coalesce.[13,14] Finally, a handful of studies have estimated D_b, instead of viscosity, by investigating the growth/evaporation kinetics of particles.[17,18,21,22] Additional uncertainties in previous estimates are also likely related to differences in the SOA composition that result from different formation conditions (e.g., chamber versus flow tube, fresh versus aged) and mass concentrations.[16] Regardless, current estimates for ν and D_b for α-pinene-derived SOA under dry conditions translate to a mixing and equilibration timescale that spans from a few minutes to several years. There appears to be a need

Received: August 28, 2020
Revised: December 14, 2020
Accepted: December 15, 2020

for novel techniques and approaches that can aid in reducing the large uncertainty in the phase state of SOA.

The phase state of SOA can influence the evolution of the particle size distribution. For SOA mass condensing into a liquidlike aerosol, vapors should partition into the entire particle volume regardless of the particle size. For condensation into a semisolid aerosol, vapors should mostly partition into the entire volume for the smaller particles but closer to the edge for the larger particles as the timescales for mixing are proportional to the square of the particle size ($\tau_{diff} = \frac{R_p^2}{\pi^2 D_b}$, where R_p is the particle radius). Hence, for the same amount of condensing SOA mass, a semisolid aerosol should promote faster diameter growth of nucleation (1−10 nm) and Aitken (10−100 nm) mode particles relative to accumulation (100−1000 nm) mode particles compared to a liquidlike aerosol and produce a narrowing of the particle size distribution with SOA formation.[23] This effect has been observed in a handful of studies. For example, in SOA formed from *n*-dodecane in a laboratory experiment, Shiraiwa et al.[3] found that, in addition to modeling the multiphase chemistry, they had to assume a semisolid SOA (D_b of 10^{-12} cm^2 s^{-1}) to explain the observed narrowing in the particle size distribution with time. Similarly, Zaveri and co-workers[17,18] found that α-pinene-derived SOA was likely to be semisolid because only a D_b between 10^{-15} and 10^{-14} cm^2 s^{-1} in their aerosol model could reproduce observations of the rapid growth of Aitken mode particles with isoprene-derived SOA. We should note that the volatility of the condensing species (C^*, effective saturation concentration)[24] can have a similar, but less pronounced, effect on the particle size distribution.[25−27] In instances where the phase state affects the evolution of the particle size distribution, these data, which are routinely measured in laboratory experiments, could be leveraged to constrain the phase state of SOA in both idealized (e.g., single VOC) and realistic (e.g., VOC mixtures, combustion emissions) model systems.

In this work, we include a treatment of the particle phase state in a detailed chemistry, thermodynamics, and microphysics model for SOA (i.e., Statistical Oxidation Model coupled to the TwO Moment Aerosol Sectional (SOM-TOMAS)) and apply this model to study the phase state of SOA formed from α-pinene ozonolysis. We show that routine environmental chamber data can be used to constrain the bulk diffusion coefficient (D_b) of SOA, requiring only measurements of the time-evolving SOA mass concentration and particle size distribution. Our work demonstrates that the particle phase state of SOA can be inferred from historical laboratory data and complement future laboratory studies and field observations of the particle phase state.

2. MATERIALS AND METHODS

2.1. Environmental Chamber Data. We modeled the SOA formation from a set of α-pinene ozonolysis experiments that are described in detail in Nah et al.[28] These experiments were chosen for several reasons. First, these experiments were characterized for vapor loss and size-dependent losses of particles to the chamber walls, inputs necessary to predict the time-varying suspended particle data. Second, they included both seeded and unseeded experiments; the unseeded experiment proved particularly useful because the modeled evolution of the particle size distribution varied substantially with the use of different D_b values and this effect was used to constrain the D_b (explained later). Third, the phase state of α-pinene-derived SOA has been extensively studied in the past and thus the results from this work could be compared with historical data.[11,13,14,16−19,29]

The experiments of Nah et al.[28] were performed in the 13 m^3 Georgia Tech Environmental Chamber (GTEC) facility, with full details provided in previous work.[30] In all experiments, 50 ppbv of α-pinene was added to a clean chamber along with 22 ppm of cyclohexane, which served as an OH scavenger and ensured that the α-pinene reacted only with O_3. Experimental conditions featured low NO_x concentrations (<1 ppbv), a temperature of 25 °C, and relative humidity of <5%. Experiments were performed either with 100 or 500 ppbv of O_3, which reacted immediately with α-pinene under dark conditions. For each O_3 level, one experiment was performed with no seed particles which resulted in homogeneous nucleation and growth of the freshly formed particles. Two other experiments were performed with low (∼1000 μm^2 cm^{-3}) and high (∼3000 μm^2 cm^{-3}) initial dry ammonium sulfate seed concentrations, where SOA condensed onto the seeds. The instrumentation used to measure the gas- and particle-phase species is summarized in Table S1.

2.2. SOM-TOMAS Model and Updates for Highly Oxygenated Organic Molecules (HOM) Formation. We used the Statistical Oxidation Model coupled to the TwO Moment Aerosol Sectional model (SOM-TOMAS) to simulate the SOA formation from α-pinene ozonolysis in environmental chamber experiments. Detailed descriptions of the SOM[31,32] and TOMAS[33,34] models can be found in previous publications. More recently, the SOM-TOMAS model was used to model SOA formation in chamber experiments performed on unburned biofuels[35] and emissions from biomass burning.[36]

The SOM tracks the chemical evolution of the VOC and its oxidation products using a two-dimensional, carbon (N_C) and oxygen (N_O) number grid. The properties of each model species (e.g., reactivity (k_{OH}), volatility (C^*)) are parameterized based on their N_C and N_O. The SOM has five adjustable parameters that govern the oxidation chemistry and thermodynamic properties of the model species: (i−iv) $p_{f,1}$−$p_{f,4}$, the yields of four functionalized products that add one, two, three, and four oxygen atoms to the carbon backbone, respectively; (v) ΔLVP, the decrease in the C^* of the model species per addition of an oxygen atom. We did not model fragmentation reactions because O_3 was the only oxidant present in the chamber experiments. The TOMAS model tracks the evolution of the aerosol number distribution and species-resolved mass distribution and simulates kinetic condensation/evaporation and coagulation. New particle formation in the nucleation experiments was specified based on the experimental data (Section S1 and Figure S1) and the SOM-TOMAS model was used to simulate vapor and size-dependent particle wall losses similar to that in previous work (Section S2). In this work, we used 60 size sections in TOMAS spanning dry diameters of 3−2000 nm.

Reaction intermediates formed during α-pinene ozonolysis (i.e., peroxy radicals) can autooxidize under low NO_x conditions to rapidly form highly oxygenated organic molecules (HOM).[37] HOM have extremely low C^* values (<10^{-4} μg m^{-3}) and high O/C ratios (∼1) and are known to contribute to new particle formation and growth.[38−40] To account for this, we added an autooxidation pathway to the SOM-TOMAS model, where the α-pinene reaction with O_3

https://dx.doi.org/10.1021/acs.est.0c05796
Environ. Sci. Technol. XXXX, XXX, XXX−XXX

directly led to the formation of HOM with a fixed molar yield (f_{HOM}) and a C* of 10^{-4} μg m^{-3}; species with volatilities this low are effectively nonvolatile. Based on the work of Jokinen et al.,[39] we used a molar yield of 3.4%, or equivalently a mass yield of 7.9%, to model HOM formation from α-pinene ozonolysis. We ensured that the sum of $p_{f,1}$ through $p_{f,4}$ and f_{HOM} was exactly equal to 1.

This version of the SOM-TOMAS model, which included functionalization reactions and formation of HOMs, was updated to account for the influence of the particle phase state on kinetic gas/particle partitioning (Section 2.4). In this version, the D_b for the SOA was specified a priori and, hereafter, this is referred to as the prescribed-D_b version.

2.3. Endogenous-D_b Model and Updates for Particle Phase Reactions. We developed a separate endogenous-D_b version of the SOM-TOMAS model in which the D_b was calculated based on the simulated, evolving chemical composition of SOA. The D_b was calculated following the semiempirical framework developed by Shiraiwa and co-workers,[29,41−43] the equations for which are described in the Supporting Information (Section S3). Briefly, the molecular weights and O/C ratios of the condensed model species were used to estimate the glass-transition temperature (T_g) for the model species and these T_gs were weighted by their mass fraction to calculate the average $T_{g,org}$ for the SOA mixture. Using a fragility parameter set to 10, we estimated the viscosity (ν) using Angell[44] and then D_b from ν using the fractional Stokes−Einstein relation.[45] A single time-evolving D_b value was calculated for all SOA and applied to all particle size sections. A separate model was developed that calculated a size-dependent D_b and was used to perform sensitivity simulations.

High-molecular-weight oligomers have been frequently observed in SOA from α-pinene ozonolysis[46,47] and are likely to exert a strong influence on the particle phase state. To account for the influence of oligomers on D_b, we included an oligomerization scheme in the endogenous-D_b model, with reversible oligomer formation and dissociation, characterized by a forward reaction rate (k_f, cm^3 molecule^{-1} s^{-1}) and reverse reaction rate (k_r, s^{-1}), respectively. Only dimer formation and dissociation were included, assumed to represent general oligomer formation. Serving as monomers, the four functionalized oxidation products, in all combinations, were allowed to form dimers and we assumed that the dimers decomposed back into the same monomer pair that the dimer was formed from. Depending on the ΔLVP, the monomers included both semivolatile and low-volatility species. HOM were excluded from oligomerization reactions since there is little evidence for HOM participating in additional particle phase reactions.[37] k_f was specified and k_r was treated as an adjustable parameter. This oligomerization scheme was similar to that described in Trump and Donahue[48] and the equations are as follows

$$\frac{dO_{i,j}}{dt} = \sum_{k}^{i_{max}} k_f \cdot M_{k,j} \cdot M_{i,j} - k_r \cdot O_{i,j} \quad (1)$$

$$\frac{dM_{i,j}}{dt} = k_r \cdot O_{i,j} - \sum_{k}^{i_{max}} k_f \cdot M_{i,j} \cdot M_{k,j} \quad (2)$$

where M and O are the monomer and dimer concentrations in the particle phase in molecules per cm^3 of particle volume, respectively; i and k are the species and j is the size bin. We also calculated the first-order loss rate of the condensing species in the particle phase to oligomerization reactions, $k^c_{i,j}$ (s^{-1}). $k^c_{i,j}$ is calculated assuming that the dimer mass is in pseudo-steady state with the monomer mass

$$k^c_{i,j} = \sum_{k}^{i_{max}} k_f \cdot M_{k,j} - k_r \cdot \frac{O_{i,j}}{M_{i,j}} \quad (3)$$

2.4. Representing the Influence of Particle Phase State on Gas/Particle Partitioning. In the SOM-TOMAS model, the influence of D_b on the kinetic gas/particle partitioning of SOA was implemented using the diffusion-reactive framework of Zaveri et al.[23] Depending on the first-order chemical loss rate ($k^c_{i,j}$) of the model species in the particle phase, the differential equations used to model the condensation and evaporation of a species i, for a polydisperse size distribution, can take on different forms. For a slow particle phase reaction ($k^c_{i,j}$ < 0.01 s^{-1})

$$\frac{dC^g_i}{dt} = -\sum_{j} 4\pi \cdot (R^p_j)^2 \cdot N^p_j \cdot K_{i,j} \left(C^g_i - \frac{C^p_{i,j}}{SOA_j} C^*_i S_j \right) \quad (4)$$

$$\frac{dC^p_{i,j}}{dt} = 4\pi \cdot (R^p_j)^2 \cdot N^p_j \cdot K_{i,j} \left(C^g_i - \frac{C^p_{i,j}}{SOA_j} C^*_i S_j \right) \quad (5)$$

where C^g_i is the gas-phase concentration of the species i in μg m^{-3}, $C^p_{i,j}$ is the particle phase concentration of the species i in size bin j in μg m^{-3}, R^p_j is the radius of the particle in size bin j in m, N^p_j is the particle number concentration in size bin j m^{-3}, $K_{i,j}$ is the overall gas-side mass transfer coefficient for species i in size bin j in m s^{-1}, SOA_j is the total SOA mass concentration in size bin j in μg m^{-3}, C^*_i is the effective saturation concentration of species i in μg m^{-3}, and S_j is the Kelvin ratio (Section S4). $K_{i,j}$ is calculated as follows:

$$\frac{1}{K_{i,j}} = \frac{1}{k^g_{i,j}} + \frac{1}{k^p_{i,j}} \left(\frac{C^*_i}{\rho_p} \right) \quad (6)$$

$$k^g_{i,j} = \frac{D^g_i \cdot FS_{i,j}}{R^p_j} \quad (7)$$

$$k^p_{i,j} = \frac{D_b}{R^p_j} \left(\frac{q_{i,j} \coth q_{i,j} - 1}{1 - Q_{i,j}} \right) \quad (8)$$

$$q_{i,j} = R^p_j \sqrt{\frac{k^c_{i,j}}{D_b}} \quad (9)$$

$$Q_{i,j} = 3 \left(\frac{q_{i,j} \coth (q_{i,j}) - 1}{q^2_{i,j}} \right) \quad (10)$$

where $k^g_{i,j}$ is the gas-side mass transfer coefficient for species i in size bin j in m s^{-1}, $k^p_{i,j}$ is the particle-side mass transfer coefficient in m s^{-1}, ρ_p is the SOA density in kg m^{-3}, $FS_{i,j}$ is the Fuchs−Sutugin correction factor (Section S4), $q_{i,j}$ is a unitless diffusion-reaction parameter for species i in size bin j, and $Q_{i,j}$ is the ratio of the average bulk concentration of species i to its concentration at the particle surface at steady state for size bin j. We should note that eq 8 shows the formulation of $k^p_{i,j}$ for a well-mixed particle where diffusion of the condensing species occurs across the entire particle radius. However, to simulate

https://dx.doi.org/10.1021/acs.est.0c05796
Environ. Sci. Technol. XXXX, XXX, XXX−XXX

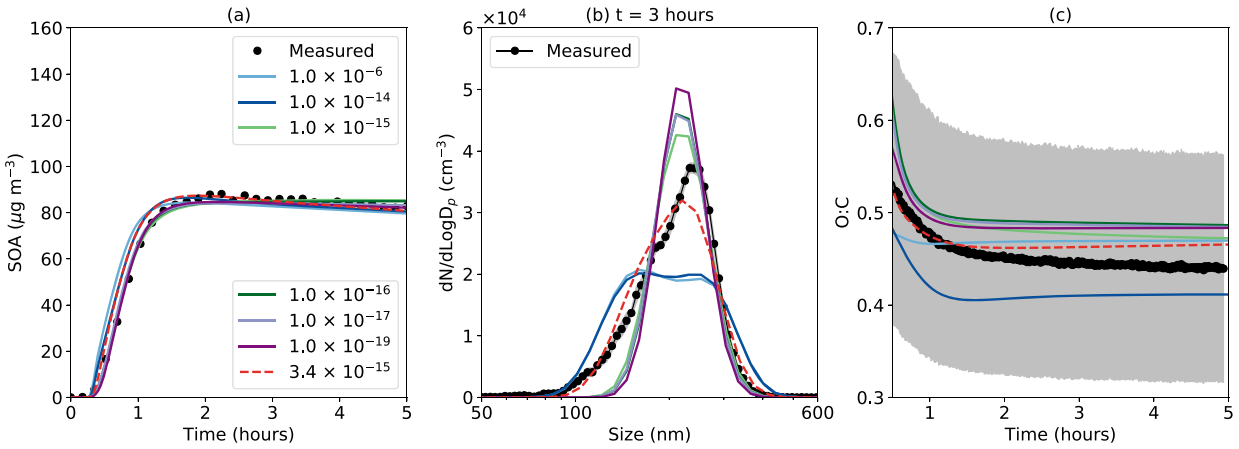

Figure 1. Results from the SOM-TOMAS model for (a) SOA mass concentration, (b) number size distribution at 3 h, and (c) O/C ratio compared to measurements for a range of prescribed-D_b ($cm^2\ s^{-1}$) values. Results are for the 500 ppbv O_3, nucleation experiment. The dashed red line shows model predictions from the optimal fit when constrained to both the SOA mass concentration and number size distribution. The O/C data are only shown 30 min after the start of the experiment because the O/C measurements are fairly uncertain in the first 30 min when the SOA mass concentrations are quite low. The gray bands in (b) and (c) depict ± 1σ.

the seeded experiments, we derived an updated formula for $k^p_{i,j}$ where the diffusion of the condensing species occurred across an organic shell around an ammonium sulfate core (derivation in Section S5). For a fast particle phase reaction ($k^c_{i,j} > 0.01\ s^{-1}$)

$$\frac{dC_i^g}{dt} = -\sum_j 4\pi\cdot(R_j^p)^2\cdot N_j^p\cdot k_{i,j}^g\left(C_i^g - \frac{C_{i,j}^p}{SOA_j Q_{i,j}} C_i^* S_j\right) \quad (11)$$

$$\frac{dC_{i,j}^p}{dt} = 4\pi\cdot(R_j^p)^2\cdot N_j^p\cdot k_{i,j}^g\left(C_i^g - \frac{C_{i,j}^p}{SOA_j Q_{i,j}} C_i^* S_j\right) \quad (12)$$

For a liquidlike aerosol when D_b is greater than 10^{-10} $cm^2\ s^{-1}$, eqs 4, 11 and 5, 12 resemble the condensation/evaporation equation expressed in the continuum regime.[49]

2.5. Simulations. The following three sets of simulations were performed to constrain the D_b of the SOA formed from α-pinene ozonolysis. First, the SOM parameters ($p_{f,1-4}$ and ΔLVP with f_{HOM} = 3.4%) were fit to reproduce the time-varying SOA mass concentrations in the nucleation experiments for a prescribed-D_b value, that ranged between 10^{-6} and 10^{-19} $cm^2\ s^{-1}$. Predictions of the SOA O/C and particle size distribution from these simulations were compared with measurements. Second, to determine an optimal fit, the SOM parameters ($p_{f,1-4}$ and ΔLVP with f_{HOM} = 3.4%) and D_b were fit to simultaneously reproduce the time-varying SOA mass concentrations and particle size distribution in the nucleation experiments. Third, using the optimal SOM parameters determined in the second set of simulations, we simulated the nucleation experiments using the endogenous-D_b model. k_f was fixed at either 10^{-24} cm^3 $molecule^{-1}\ s^{-1}$ (faster reaction) or 10^{-25} cm^3 $molecule^{-1}\ s^{-1}$ (slower reaction), and k_r was adjusted to reproduce the time-varying SOA mass concentrations. In essence, we determined a k_f–k_r pair to optimize oligomer formation that then approximately produced the same D_b as that determined in the optimal fit. Finally, the endogenous-D_b model was used to study the impact of a size-dependent D_b on the evolution of the particle size distribution. For the first two sets, the simulations and their evaluations were done separately for the 100 and 500 ppbv O_3 experiments. The first set was also applied to simulate SOA formation in the seeded experiments. All model predictions were compared to measurements for the suspended aerosol since the model inherently accounted for size-dependent losses of particles and losses of vapors to the chamber walls.

3. RESULTS

Results from application of the prescribed-D_b version of the SOM-TOMAS model to the α-pinene ozonolysis nucleation experiment with 500 ppbv O_3 are presented in Figure 1. A unique set of SOM parameters ($p_{f,1-4}$ and ΔLVP with f_{HOM} = 3.4%) was developed for each prescribed-D_b that reproduced the time-varying SOA mass concentrations (Figure 1a; solid lines); the SOM parameters from these fits are tabulated in Table S2. However, the use of different D_b values produced a significantly different evolution of the particle number size distribution. In Figure 1b, we compare the predicted and measured number size distribution at 3 h after the start of the ozonolysis experiment. The simulations showed that the use of a higher D_b (>10^{-14} $cm^2\ s^{-1}$) produced a broader distribution while a lower D_b (<10^{-15} $cm^2\ s^{-1}$) produced a narrower distribution. As the D_b values were varied between 10^{-14} and 10^{-15} $cm^2\ s^{-1}$, the simulations produced a distribution that progressively transitioned between the broad and narrow number size distributions observed at the two extremes (Figure S2). These results can be explained by understanding the size-resolved dynamics of SOA condensation that changed with the different prescribed-D_b values.

Smaller particles exhibit shorter timescales for bulk particle phase diffusion and hence condensation of SOA onto nucleation and Aitken mode sizes was not significantly affected by changes in D_b. For instance, for a 10 nm particle, τ_{diff} varies between 2.5 and 25 s for D_b values between 10^{-14} and 10^{-15} $cm^2\ s^{-1}$, respectively. In contrast, larger particles exhibit longer timescales for bulk diffusion, which resulted in accumulation of the species at the particle surface and limited additional condensation for accumulation mode particles with the use of a lower D_b. For a 200 nm particle, τ_{diff} varies between 17 min and 3 h for D_b values between 10^{-14} and 10^{-15} $cm^2\ s^{-1}$, respectively. Furthermore, the use of a lower D_b resulted in

https://dx.doi.org/10.1021/acs.est.0c05796
Environ. Sci. Technol. XXXX, XXX, XXX−XXX

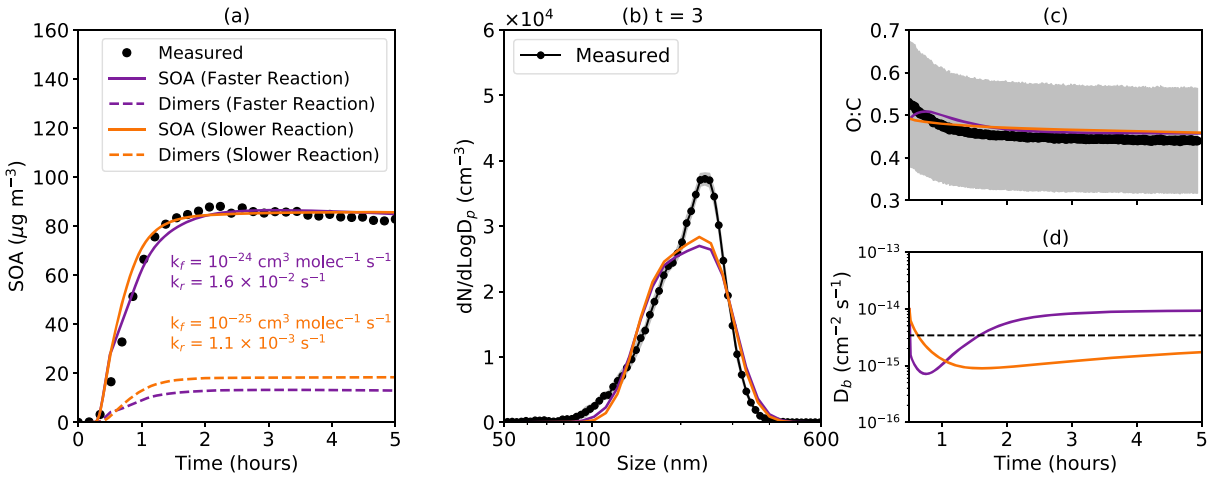

Figure 2. Results from the endogenous-D_b version of the SOM-TOMAS model for (a) SOA mass concentration, (b) number size distribution at 3 h, and (c) O/C ratio compared to measurements. (d) Model predictions of the time-varying D_b. Results are for the 500 ppbv O_3, nucleation experiment. Both the slower-reacting (orange lines) and faster-reacting (purple lines) cases use the SOM parameters from the optimal D_b fit in Figure 1 ($p_{f,1-4}$, ΔLVP, f_{HOM} = 3.4%) but with different oligomer formation and dissociation rates. The O/C data are only shown 30 min after the start of the experiment because the O/C measurements are fairly uncertain in the first 30 min when the SOA mass concentrations are quite low. The gray bands in (b) and (c) depict ± 1σ.

enhanced formation of lower-volatility species, which were necessary to reproduce the observed SOA formation under bulk diffusion limitations (Figure S3). Lower-volatility species, regardless of the D_b, condense irreversibly on all particle sizes with the diameter growth rate having no dependence on particle size in the kinetic regime and slowing with increasing size in the transition regime. Overall, a lower D_b resulted in a relatively faster diameter growth rate for the smaller particles compared to the larger particles and this produced the distinct number size distributions shown in Figure 1b. This finding is generally consistent with previous theoretical and experimental studies that have observed a similar narrowing in the number size distribution with the use of a lower D_b and/or lower C^* of the condensing species.[17,18,23,26,50−52]

The prescribed-D_b simulations indicated that a D_b value between 10^{-15} and 10^{-14} cm^2 s^{-1}, a range that reflects a semisolid particle phase state, might reproduce the observed evolution in the number size distribution. When the SOM-TOMAS model was used to fit both the SOM and D_b to the time-varying SOA mass concentrations and number size distribution, the fitting produced a D_b of 3.4×10^{-15} cm^2 s^{-1}; model predictions based on this fit are shown as a dashed red line in Figure 1. Similar comparisons as shown in Figure 1b at other times (e.g., 0.5, 1, and 5 h) are presented in the Supporting Information(Figure S4), and these support the findings presented here.

Simulations based on parameters for the different D_b values did not seem to produce large differences in the SOA O/C ratio (Figure 1c), and the predictions were well within the bounds of the measurements. Model predictions with D_b values equal to or smaller than the optimal value (3.4×10^{-15} cm^2 s^{-1}) reproduced the general trend in the observed SOA O/C ratio: an initial decrease and a gradual flattening over time. We concluded that the SOA O/C data did not contain information that could be used to constrain the D_b further and hence the O/C data were not used as part of the fitting process. However, model predictions of the SOA O/C were found to be sensitive to HOM production. Simulations performed without the formation of HOM, but with fits that reproduced the time-varying SOA mass concentrations, resulted in an average SOA O/C of 0.39 between 2 and 5 h. Although still within the uncertainty range in the measurements, this was lower than the mean measured SOA O/C of 0.44 during the same time period. This suggests the need for HOM to be explicitly accounted for in models to ensure accurate predictions of SOA O/C.

Previous work has found that condensation of lower-volatility material ($C^* < 10^{-4}$ μg m^{-3}), including HOM, can produce a similar narrowing in the particle size distribution,[3,25,26] as seen in Figure 1b with the use of a lower D_b. We investigated if the observations could only be explained by the production of low-volatility material (HOM in this case), but assuming a liquidlike SOA. For a D_b of 10^{-6} cm^2 s^{-1}, we determined SOM parameters ($p_{f,1-4}$, ΔLVP) for several predefined values of f_{HOM} (3.4, 7, 10, and 20%) that reproduced the time-varying SOA mass concentrations. We found that while an increase in the production of HOM produced slight variations in the number size distribution at 3 h, none of the model predictions compared well with the observations (Figure S5). Further, the use of a larger f_{HOM} resulted in a relatively weaker comparison for the SOA mass concentration and O/C ratio. For the largest f_{HOM} (20%), the model formed SOA too rapidly and overpredicted the SOA O/C. These simulation results suggest that the SOA volatility was much less influential than the phase state in controlling the evolution of the particle size distribution and provided further evidence that α-pinene-derived SOA was semisolid with a D_b between 10^{-14} and 10^{-15} cm^2 s^{-1}.

In Figure 1, we chose not to present results from simulations performed with D_b values between 10^{-6} and 10^{-14} cm^2 s^{-1} because the model predictions for SOA mass concentration and number size distribution were nearly identical for any D_b between those bounds. Differences in model predictions of the number size distribution started to appear at D_b values lower than 10^{-14} cm^2 s^{-1}. While the literature has defined organic material with a D_b of 10^{-14} cm^2 s^{-1} and up to a D_b of 10^{-10} cm^2 s^{-1} as semisolid,[53] these D_b values appeared to mimic the model response with a D_b strictly in the liquid range (>10^{-10} cm^2 s^{-1}). This result suggests that the SOA condensation in nucleation experiments may not necessarily be limited by the

https://dx.doi.org/10.1021/acs.est.0c05796
Environ. Sci. Technol. XXXX, XXX, XXX−XXX

Table 1. Estimates of D_b from This Work Compared to Historical Estimates under Dry Conditions for α-Pinene-Derived SOA[a]

reference	oxidant	SOA formed in	RH (%)	max. SOA mass conc. ($\mu g\ m^{-3}$)	D_b ($cm^2\ s^{-1}$)	D_b estimated using
this work	O_3	13 m^3 chamber at <5% RH	<5	60−80	$1-7 \times 10^{-15}$	evolution of the particle size distribution
Zaveri et al.[18]	OH	10.6 m^3 chamber at 32% RH	32	110	2.5×10^{-15}	growth of SOA on different sized particles
Abramson et al.[19]	O_3	0.1 m^3 chamber at ∼0% RH	∼0	NM[b]	2.5×10^{-17}	evaporation of pyrene trapped inside SOA
Zhou et al.[20]	O_3	flow tube at <5% RH	∼0	NM[b]	2×10^{-14}	oxidation of benzo[a]pyrene trapped inside SOA
Renbaum-Wolff et al.[11]	O_3	flow tube at <5% RH	0−30	50	$<10^{-17}$	flow properties of large SOA particles
Pajunoja et al.[13]	O_3	6 m^3 chamber at 35% RH	<20	3−15	$>3 \times 10^{-21}$	coalescence time of individual particles
	OH				$<3 \times 10^{-21}$	
Zhang et al.[14]	O_3	flow tube at <5% RH	<5	70	6×10^{-18}	change in particle shape factor
Grayson et al.[16]	O_3	flow tube at <5% RH	0.5	14 000	$2 \times 10^{-15}-7 \times 10^{-14}$	flow properties of large SOA particles
		chamber at <5% RH	0.5	121	$6 \times 10^{-17}-5 \times 10^{-15}$	

[a]When not directly available, the D_b was estimated from the viscosity using the Stokes−Einstein equation. [b]NM = not mentioned.

particle phase state even when the SOA D_b is near the upper end ($10^{-10}-10^{-14}$ $cm^2\ s^{-1}$) of the semisolid range ($10^{-10}-10^{-18}$ $cm^2\ s^{-1}$). The "critical" D_b where the number size distribution evolution began to change (10^{-14} $cm^2\ s^{-1}$, in this case) was likely to be lower in the nucleation experiment because the kinetics of SOA condensation was primarily driven by growth of nucleation and Aitken mode particles that are less susceptible to the effects of bulk diffusion. If the experiments were to be performed with absorbing seed particles in the accumulation mode that had the same D_b as the condensing SOA, the critical D_b would have very well been much higher ($>10^{-14}$ $cm^2\ s^{-1}$).

The SOM-TOMAS model was applied to another α-pinene ozonolysis nucleation experiment performed at lower initial O_3 concentrations (100 ppbv; Figure S6). The findings from this application were very similar to those discussed above and an optimal D_b of 4.4×10^{-15} $cm^2\ s^{-1}$ was determined based on simultaneously fitting the SOA mass concentration and the evolution of the number size distribution. We explored the sensitivity in the optimal D_b by performing simulations and fits with the vapor wall loss rate, size-dependent particle wall loss rate, and f_{HOM}, all doubled and halved. This sensitivity analysis, presented in Figures S7−S9 for the 500 ppbv O_3 experiment, suggested that the optimal D_b was tightly constrained between 1.4×10^{-15} and 7.1×10^{-15} $cm^2\ s^{-1}$ for the uncertainty in these three inputs.

The technique used to constrain D_b in the nucleation experiments did not work with the seeded experiments due to the invariability in the predicted number size distribution with different prescribed-D_b values. We attributed this to the relatively uniform SOA coating thickness around the ammonium sulfate core in these particular seeded experiments. The simulation results are shown in Figures S10−S12, and the results are described in Section S6.

The results from application of the endogenous-D_b version of the SOM-TOMAS model—where D_b was calculated from predictions of the SOA composition—to the α-pinene ozonolysis nucleation experiment with 500 ppbv O_3 are presented in Figure 2. To note, we used the optimal SOM parameters from Figure 1 and determined a k_f−k_r pair that reproduced the time-varying SOA mass concentrations. This, in essence, optimized the oligomer production to approximately reproduce the same SOA D_b as the optimal D_b identified in Figure 1.

The fitting resulted in k_r values of 1.1×10^{-3} s^{-1} and 1.6×10^{-2} s^{-1} for the slower and faster oligomerization schemes, respectively, and produced very similar predictions in the SOA O/C (Figure 2c) that agreed well with the measurements. Increasing the k_f to values larger than 10^{-24} cm^3 molecule s^{-1} produced too low of an initial D_b ($<10^{-19}$ $cm^2\ s^{-1}$) from a large oligomer fraction to condense any oxidation products apart from the HOM. A k_f value lower than 10^{-25} cm^3 molecule s^{-1} (and down to ∼0) produced too high of an initial D_b ($>10^{-13}$ $cm^2\ s^{-1}$) from very few oligomers to agree with the evolution in the number size distribution. The model-measurement comparison for the SOA mass concentration and the number size distribution seemed to bound the k_f−k_r ranges, which were generally found to be consistent with those reported in the literature.[54−56] The oligomer mass concentrations and temporal profiles were consistent between the slower and faster schemes and the oligomers were between 15 and 21% of the total SOA by the end of the experiment. This oligomer mass fraction, although slightly on the lower side, was consistent with previously measured oligomer fractions in α-pinene ozonolysis SOA in chamber and flow tube experiments (30−75%).[18,46] In contrast to the results shown in Figure 1, where D_b was prescribed and remained constant throughout the experiment, D_b, shown in Figure 2d, changed with time but remained between 10^{-15} and 10^{-14} $cm^2\ s^{-1}$. The average model-predicted D_b values during the first two hours of the simulations were 2.4×10^{-15} and 1.5×10^{-15} $cm^2\ s^{-1}$ for the slower and faster oligomerization schemes, respectively. In summary, by knowing the SOA D_b from earlier simulations and using the semiempirical approach proposed by Shiraiwa and co-workers,[29,41−43] we were able to constrain the formation of high-molecular-weight oligomers that were contributing to the semisolid phase state of SOA. This finding would need to be validated in the future with explicit measurements of oligomers in SOA.

Additional simulations were performed with the size-dependent, endogenous-D_b model to study its impacts on SOA formation and the particle size distribution; the simulation results are shown in Figure S13. For the k_f−k_r pairs that reproduced the SOA mass concentrations, we found that these simulations failed to reproduce observations of the

https://dx.doi.org/10.1021/acs.est.0c05796
Environ. Sci. Technol. XXXX, XXX, XXX−XXX

particle size distribution. For the slower k_f simulation, the size-dependent D_b favored SOA condensation onto smaller particle sizes and resulted in a very narrow particle size distribution. For the faster k_f simulation, the SOA seemed to condense on all sizes to produce a very broad particle size distribution. Although the slower and faster k_f simulations might give the impression that they bound the model's particle size distribution response, the model responded nonlinearly to all intermediate k_f and k_r values (not shown) with the actual response being sensitive to the size- and time-dependent HOM, monomer, and dimer composition. In this work, we were unable to model the size-dependent D_b while reconciling both the mass and size distribution measurements. Future work, informed by more recent studies,[63,64] should aim to study this aspect in more detail.

4. DISCUSSION

We used a chemistry, thermodynamics, and microphysics model to simulate the formation of fresh SOA formed from α-pinene ozonolysis in two nucleation experiments.[28] We discovered that we were able to explain the SOA production and the evolution in the particle size distribution only if we assumed a semisolid SOA with a D_b between 1×10^{-15} and 7×10^{-15} cm^2 s^{-1}. This D_b was compared with historical D_b values estimated for α-pinene-derived SOA formed and/or sampled under dry conditions (RH < 30%) in Table 1. The D_b range estimated in this work agreed with the value estimated by Zaveri et al.[18] (2.5×10^{-15} cm^2 s^{-1}) who used a similar thermodynamic approach to constrain D_b, based on the varying growth rates observed for particles of different sizes. However, the D_b values in our work were found to be near the upper end of the observational range in Table 1 (10^{-21}–10^{-14} cm^2 s^{-1}), which was primarily inferred from measurements of viscosity. Furthermore, the Stokes–Einstein equation that allows for calculation of D_b from viscosity has been shown to underestimate D_b for highly viscous material.[45] Hence, our work tentatively suggests that the D_b for α-pinene-derived SOA inferred from the thermodynamic behavior might be much larger than that estimated in the literature based on its viscosity. While we demonstrate a novel technique to constrain D_b using historical chamber data, additional work is needed to reconcile the large differences in D_b and viscosity previously observed for this model system. Future work to constrain the particle phase state could be further complicated by recent observations of liquid–liquid phase separation at high relative humidity[43] and the formation of surface crusts with chemical aging.[6]

Water uptake at subsaturated and more atmospherically relevant conditions is known to have a plasticizing effect[57] that has been shown to dramatically alter the phase state of SOA.[15,58,59] Water vapor can also influence the oxidation chemistry to change the molecular composition of SOA and thus its phase state.[12] In two recent papers that compiled phase state data for SOA from different precursors,[10,29] a change in RH from <5 to ∼90% decreased the SOA viscosity by 7–10 orders of magnitude. DeRieux et al.[29] showed that the semiempirical framework used in this work to calculate viscosity from the SOA composition was generally able to reproduce the observed changes in viscosity with RH for SOA derived from α-pinene, isoprene, and toluene. The D_b for α-pinene-derived SOA was estimated in this work based on chamber experiments performed under dry conditions (RH < 5%). Hence, the models developed in this work, including the endogenous-D_b version, need to be used to explore the phase state of SOA in experiments performed under wet conditions. Since particle size distribution data are routinely collected during laboratory experiments, our methods could easily be extended to historical unseeded data and potentially to seeded data.

The phase state has also been shown to affect the kinetics of SOA evaporation when perturbed with dilution, heating, or removing vapors in equilibrium with the SOA.[21,22,46–48,60] To study the kinetics of SOA evaporation, we performed additional simulations with the SOA found at the end of the nucleation experiments. In these evaporation simulations, we instantaneously removed any vapors in the simulated chamber (but not particles) and studied the multihour evolution of the remaining SOA with the SOM-TOMAS model, where the D_b was prescribed (3.4×10^{-15} cm^2 s^{-1}) and or calculated endogenously from the chemical composition. The results from these simulations are shown in Figure 3, where we compare the normalized evolution of remaining SOA volume with historical data for SOA studies under dry conditions (different experiments than used for our simulations).[22,47] The model with the prescribed-D_b overestimated both the rate and net loss of SOA while the endogenous models appeared to bracket the observational range. As the D_b value for the SOA was roughly similar between all three simulations, these results suggest that models need to account for oligomers, in addition to representing the phase state and volatility distribution accurately, to reproduce the observed evaporation kinetics. Furthermore, this supports the general approach used in this work to first determine a D_b using a prescribed-D_b model and then using an endogenous-D_b model to constrain oligomer formation and dissociation. It is important to note that the SOA observations in Figure 3 were collated from several different studies with substantial differences in experimental details. Regardless, observations of the evaporation of SOA with dilution or heating could provide additional constraints on the SOA composition and properties when used in conjunction with detailed process-based models.[61]

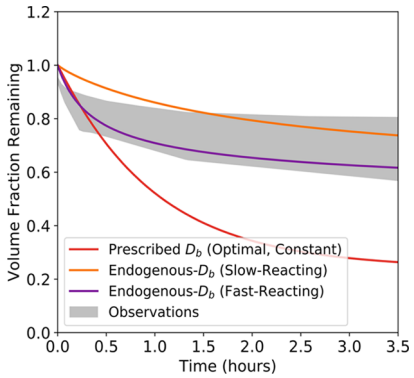

Figure 3. Simulated evaporation of the end-of-experiment SOA for the SOM-TOMAS model with $D_b = 3.4 \times 10^{-15}$ cm^2 s^{-1} and the endogenous-D_b version of the model with slower and faster oligomerization rates. The observational range is adapted from the following studies: Sato et al.,[47] Grieshop et al.,[60] Vaden et al.,[21] Yli-Juuti et al.,[22] and D'Ambro et al.[46]

Particle phase state is rarely, if at all, explicitly accounted for in aerosol modules present in atmospheric models to simulate the formulation and evolution of SOA or organic aerosol. This work suggests that a semisolid SOA, which is likely to be

https://dx.doi.org/10.1021/acs.est.0c05796
Environ. Sci. Technol. XXXX, XXX, XXX–XXX

encountered at higher latitudes and altitudes,[41] can have substantive effects on the evolution of the aerosol size distribution and subsequently exert an influence on aerosol–climate and aerosol–health interactions. We advocate for an explicit treatment of particle phase state in atmospheric models.

■ ASSOCIATED CONTENT

Supporting Information

The Supporting Information is available free of charge at https://pubs.acs.org/doi/10.1021/acs.est.0c05796.

New particle formation, chamber wall losses, phase state-specific derivations and equations used in the SOM-TOMAS model, and results from additional simulations (PDF)

■ AUTHOR INFORMATION

Corresponding Author

Shantanu H. Jathar − *Department of Mechanical Engineering, Colorado State University, Fort Collins, Colorado 80523, United States;* orcid.org/0000-0003-4106-2358; Email: shantanu.jathar@colostate.edu

Authors

Yicong He − *Department of Mechanical Engineering, Colorado State University, Fort Collins, Colorado 80523, United States*

Ali Akherati − *Department of Mechanical Engineering, Colorado State University, Fort Collins, Colorado 80523, United States*

Theodora Nah − *School of Energy and Environment and State Key Laboratory of Marine Pollution, City University of Hong Kong, Hong Kong, China;* orcid.org/0000-0002-8755-6153

Nga L. Ng − *School of Chemical and Biomolecular Engineering, Georgia Institute of Technology, Atlanta, Georgia 30332, United States; School of Earth and Atmospheric Sciences and School of Civil and Environmental Engineering, Georgia Institute of Technology, Atlanta, Georgia 30332, United States;* orcid.org/0000-0001-8460-4765

Lauren A. Garofalo − *Department of Chemistry, Colorado State University, Fort Collins, Colorado 80523, United States;* orcid.org/0000-0001-7593-2580

Delphine K. Farmer − *Department of Chemistry, Colorado State University, Fort Collins, Colorado 80523, United States;* orcid.org/0000-0002-6470-9970

Manabu Shiraiwa − *Department of Chemistry, University of California, Irvine, Irvine, California 92697, United States;* orcid.org/0000-0003-2532-5373

Rahul A. Zaveri − *Atmospheric Sciences and Global Change Division, Pacific Northwest National Laboratory, Richland, Washington 99354, United States;* orcid.org/0000-0001-9874-8807

Christopher D. Cappa − *Department of Civil and Environmental Engineering, University of California Davis, Davis, California 95616, United States*

Jeffrey R. Pierce − *Department of Atmospheric Science, Colorado State University, Fort Collins, Colorado 80523, United States;* orcid.org/0000-0002-4241-838X

Complete contact information is available at: https://pubs.acs.org/10.1021/acs.est.0c05796

Author Contributions

Y.H. and S.H.J. designed the modeling study. Y.H. and A.A. developed the model. Y.H. performed the simulations and analyzed the data along with S.H.J. T.N. and N.L.N. provided the experimental data. L.A.G. and D.K.F. analyzed the HR-AMS data to estimate SOA O/C. R.A.Z. and J.R.P. supported the model development and analysis. M.S. and C.D.C. helped review the manuscript. Y.H. and S.H.J. wrote the paper with contributions from all co-authors.

Notes

The authors declare no competing financial interest.

Simulation and measurement data used in this work are permanently archived at the following link: http://dx.doi.org/10.25675/10217/219459.

■ ACKNOWLEDGMENTS

This work was supported by the U.S. Department of Energy (DOE), Office of Science (DE-SC0017975, DE-SC0018349), National Oceanic and Atmospheric Administration (NA17OAR4310003 and NA17OAR4310001), Colorado Energy Research Collaboratory (37-2018), National Science Foundation (AGS-1455588), and the U.S. Environmental Protection Agency (RD-83540301). R.A.Z. acknowledges support from the Office of Science of the U.S. DOE as part of the Atmospheric System Research program at Pacific Northwest National Laboratory (PNNL); PNNL is operated for DOE by Battelle Memorial Institute under contract DE-AC05-76RL01830.

■ REFERENCES

(1) Jimenez, J. L.; Canagaratna, M. R.; Donahue, N. M.; Prevot, A. S. H.; Zhang, Q.; Kroll, J. H.; DeCarlo, P. F.; Allan, J. D.; Coe, H.; Ng, N. L.; Aiken, A. C.; Docherty, K. S.; Ulbrich, I. M.; Grieshop, A. P.; Robinson, A. L.; Duplissy, J.; Smith, J. D.; Wilson, K. R.; Lanz, V. A.; Hueglin, C.; Sun, Y. L.; Tian, J.; Laaksonen, A.; Raatikainen, T.; Rautiainen, J.; Vaattovaara, P.; Ehn, M.; Kulmala, M.; Tomlinson, J. M.; Collins, D. R.; Cubison, M. J.; Dunlea, E. J.; Huffman, J. A.; Onasch, T. B.; Alfarra, M. R.; Williams, P. I.; Bower, K.; Kondo, Y.; Schneider, J.; Drewnick, F.; Borrmann, S.; Weimer, S.; Demerjian, K.; Salcedo, D.; Cottrell, L.; Griffin, R.; Takami, A.; Miyoshi, T.; Hatakeyama, S.; Shimono, A.; Sun, J. Y.; Zhang, Y. M.; Dzepina, K.; Kimmel, J. R.; Sueper, D.; Jayne, J. T.; Herndon, S. C.; Trimborn, A. M.; Williams, L. R.; Wood, E. C.; Middlebrook, A. M.; Kolb, C. E.; Baltensperger, U.; Worsnop, D. R. Evolution of Organic Aerosols in the Atmosphere. *Science* **2009**, *326*, 1525−1529.

(2) Fuzzi, S.; Baltensperger, U.; Carslaw, K.; Decesari, S.; Denier van der Gon, H.; Facchini, M. C.; Fowler, D.; Koren, I.; Langford, B.; Lohmann, U.; Nemitz, E.; Pandis, S.; Riipinen, I.; Rudich, Y.; Schaap, M.; Slowik, J. G.; Spracklen, D. V.; Vignati, E.; Wild, M.; Williams, M.; Gilardoni, S. Particulate Matter, Air Quality and Climate: Lessons Learned and Future Needs. *Atmos. Chem. Phys.* **2015**, *15*, 8217−8299.

(3) Shiraiwa, M.; Seinfeld, J. H. Equilibration Timescale of Atmospheric Secondary Organic Aerosol Partitioning. *Geophys. Res. Lett.* **2012**, *39*, No. L24801.

(4) Shiraiwa, M.; Ammann, M.; Koop, T.; Pöschl, U. Gas Uptake and Chemical Aging of Semisolid Organic Aerosol Particles. *Proc. Natl. Acad. Sci. U.S.A.* **2011**, *108*, 11003−11008.

(5) Shrivastava, M.; Cappa, C. D.; Fan, J.; Goldstein, A. H.; Guenther, A. B.; Jimenez, J. L.; Kuang, C.; Laskin, A.; Martin, S. T.; Ng, N. L.; et al. Recent Advances in Understanding Secondary Organic Aerosol: Implications for Global Climate Forcing. *Rev. Geophys.* **2017**, *55*, 509−559.

(6) Zhou, S.; Hwang, B. C. H.; Lakey, P. S. J.; Zuend, A.; Abbatt, J. P. D.; Shiraiwa, M. Multiphase Reactivity of Polycyclic Aromatic Hydrocarbons Is Driven by Phase Separation and Diffusion Limitations. *Proc. Natl. Acad. Sci. U.S.A.* **2019**, *116*, 11658−11663.

(7) Murray, B. J.; Wilson, T. W.; Dobbie, S.; Cui, Z.; Al-Jumur, S. M. R. K.; Möhler, O.; Schnaiter, M.; Wagner, R.; Benz, S.; Niemand, M.; Saathoff, H.; Ebert, V.; Wagner, S.; Kärcher, B. Heterogeneous Nucleation of Ice Particles on Glassy Aerosols under Cirrus Conditions. *Nat. Geosci.* **2010**, *3*, 233−237.
(8) Wang, B.; Laskin, A.; Roedel, T.; Gilles, M. K.; Moffet, R. C.; Tivanski, A. V.; Knopf, D. A. Heterogeneous Ice Nucleation and Water Uptake by Field-Collected Atmospheric Particles below 273 K. *J. Geophys. Res.: Atmos.* **2012**, *117*, No. D00V19.
(9) Berkemeier, T.; Shiraiwa, M.; Pöschl, U.; Koop, T. Competition between Water Uptake and Ice Nucleation by Glassy Organic Aerosol Particles. *Atmos. Chem. Phys.* **2014**, *14*, 12513−12531.
(10) Reid, J. P.; Bertram, A. K.; Topping, D. O.; Laskin, A.; Martin, S. T.; Petters, M. D.; Pope, F. D.; Rovelli, G. The Viscosity of Atmospherically Relevant Organic Particles. *Nat. Commun.* **2018**, *9*, No. 956.
(11) Renbaum-Wolff, L.; Grayson, J. W.; Bertram, A. K. Technical Note: New Methodology for Measuring Viscosities in Small Volumes Characteristic of Environmental Chamber Particle Samples. *Atmos. Chem. Phys.* **2013**, *13*, 791−802.
(12) Kidd, C.; Perraud, V.; Wingen, L. M.; Finlayson-Pitts, B. J. Integrating Phase and Composition of Secondary Organic Aerosol from the Ozonolysis of α-Pinene. *Proc. Natl. Acad. Sci. U.S.A.* **2014**, *111*, 7552−7557.
(13) Pajunoja, A.; Malila, J.; Hao, L.; Joutsensaari, J.; Lehtinen, K. E. J.; Virtanen, A. Estimating the Viscosity Range of SOA Particles Based on Their Coalescence Time. *Aerosol Sci. Technol.* **2014**, *48*, i−iv.
(14) Zhang, X.; McVay, R. C.; Huang, D. D.; Dalleska, N. F.; Aumont, B.; Flagan, R. C.; Seinfeld, J. H. Formation and Evolution of Molecular Products in α-Pinene Secondary Organic Aerosol. *Proc. Natl. Acad. Sci. U.S.A.* **2015**, *112*, 14168−14173.
(15) Bateman, A. P.; Bertram, A. K.; Martin, S. T. Hygroscopic Influence on the Semisolid-to-Liquid Transition of Secondary Organic Materials. *J. Phys. Chem. A* **2015**, *119*, 4386−4395.
(16) Grayson, J. W.; Zhang, Y.; Mutzel, A.; Renbaum-Wolff, L.; Böge, O.; Kamal, S.; Herrmann, H.; Martin, S. T.; Bertram, A. K. Effect of Varying Experimental Conditions on the Viscosity of α-Pinene Derived Secondary Organic Material. *Atmos. Chem. Phys.* **2016**, *16*, 6027−6040.
(17) Zaveri, R. A.; Shilling, J. E.; Zelenyuk, A.; Liu, J.; Bell, D. M.; D'Ambro, E. L.; Gaston, C. J.; Thornton, J. A.; Laskin, A.; Lin, P.; Wilson, J.; Easter, R. C.; Wang, J.; Bertram, A. K.; Martin, S. T.; Seinfeld, J. H.; Worsnop, D. R. Growth Kinetics and Size Distribution Dynamics of Viscous Secondary Organic Aerosol. *Environ. Sci. Technol.* **2018**, *52*, 1191−1199.
(18) Zaveri, R. A.; Shilling, J. E.; Zelenyuk, A.; Zawadowicz, M. A.; Suski, K.; China, S.; Bell, D. M.; Veghte, D.; Laskin, A. Particle-Phase Diffusion Modulates Partitioning of Semivolatile Organic Compounds to Aged Secondary Organic Aerosol. *Environ. Sci. Technol.* **2020**, *54*, 2595−2605.
(19) Abramson, E.; Imre, D.; Beránek, J.; Wilson, J.; Zelenyuk, A. Experimental Determination of Chemical Diffusion within Secondary Organic Aerosol Particles. *Phys. Chem. Chem. Phys.* **2013**, *15*, 2983−2991.
(20) Zhou, S.; Shiraiwa, M.; McWhinney, R. D.; Pöschl, U.; Abbatt, J. P. D. Kinetic Limitations in Gas-Particle Reactions Arising from Slow Diffusion in Secondary Organic Aerosol. *Faraday Discuss.* **2013**, *165*, 391−406.
(21) Vaden, T. D.; Imre, D.; Beránek, J.; Shrivastava, M.; Zelenyuk, A. Evaporation Kinetics and Phase of Laboratory and Ambient Secondary Organic Aerosol. *Proc. Natl. Acad. Sci. U.S. A.* **2011**, *108*, 2190−2195.
(22) Yli-Juuti, T.; Pajunoja, A.; Tikkanen, O.; Buchholz, A.; Faiola, C.; Väisänen, O.; Hao, L.; Kari, E.; Peräkylä, O.; Garmash, O.; Shiraiwa, M.; Ehn, M.; Lehtinen, K.; Virtanen, A. Factors Controlling the Evaporation of Secondary Organic Aerosol from α-pinene Ozonolysis. *Geophys. Res. Lett.* **2017**, *44*, 2562−2570.
(23) Zaveri, R. A.; Easter, R. C.; Shilling, J. E.; Seinfeld, J. H. Modeling Kinetic Partitioning of Secondary Organic Aerosol and Size Distribution Dynamics: Representing Effects of Volatility, Phase State, and Particle-Phase Reaction. *Atmos. Chem. Phys.* **2014**, *14*, 5153−5181.
(24) Donahue, N. M.; Robinson, A. L.; Stanier, C. O.; Pandis, S. N. Coupled Partitioning, Dilution, and Chemical Aging of Semivolatile Organics. *Environ. Sci. Technol.* **2006**, *40*, 2635−2643.
(25) Riipinen, I.; Pierce, J. R.; Yli-Juuti, T.; Nieminen, T.; Häkkinen, S.; Ehn, M.; Junninen, H.; Lehtipalo, K.; Petäjä, T.; Slowik, J.; Chang, R.; Shantz, N. C.; Abbatt, J.; Leaitch, W. R.; Kerminen, V.-M.; Worsnop, D. R.; Pandis, S. N.; Donahue, N. M.; Kulmala, M. Organic Condensation: A Vital Link Connecting Aerosol Formation to Cloud Condensation Nuclei (CCN) Concentrations. *Atmos. Chem. Phys.* **2011**, *11*, 3865−3878.
(26) Pierce, J. R.; Riipinen, I.; Kulmala, M.; Ehn, M.; Petäjä, T.; Junninen, H.; Worsnop, D. R.; Donahue, N. M. Quantification of the Volatility of Secondary Organic Compounds in Ultrafine Particles during Nucleation Events. *Atmos. Chem. Phys.* **2011**, *11*, 9019−9036.
(27) Tröstl, J.; Chuang, W. K.; Gordon, H.; Heinritzi, M.; Yan, C.; Molteni, U.; Ahlm, L.; Frege, C.; Bianchi, F.; Wagner, R.; Simon, M.; Lehtipalo, K.; Williamson, C.; Craven, J. S.; Duplissy, J.; Adamov, A.; Almeida, J.; Bernhammer, A.-K.; Breitenlechner, M.; Brilke, S.; Dias, A.; Ehrhart, S.; Flagan, R. C.; Franchin, A.; Fuchs, C.; Guida, R.; Gysel, M.; Hansel, A.; Hoyle, C. R.; Jokinen, T.; Junninen, H.; Kangasluoma, J.; Keskinen, H.; Kim, J.; Krapf, M.; Kürten, A.; Laaksonen, A.; Lawler, M.; Leiminger, M.; Mathot, S.; Möhler, O.; Nieminen, T.; Onnela, A.; Petäjä, T.; Piel, F. M.; Miettinen, P.; Rissanen, M. P.; Rondo, L.; Sarnela, N.; Schobesberger, S.; Sengupta, K.; Sipilä, M.; Smith, J. N.; Steiner, G.; Tomè, A.; Virtanen, A.; Wagner, A. C.; Weingartner, E.; Wimmer, D.; Winkler, P. M.; Ye, P.; Carslaw, K. S.; Curtius, J.; Dommen, J.; Kirkby, J.; Kulmala, M.; Riipinen, I.; Worsnop, D. R.; Donahue, N. M.; Baltensperger, U. The Role of Low-Volatility Organic Compounds in Initial Particle Growth in the Atmosphere. *Nature* **2016**, *533*, 527−531.
(28) Nah, T.; McVay, R. C.; Zhang, X.; Boyd, C. M.; Seinfeld, J. H.; Ng, N. L. Influence of Seed Aerosol Surface Area and Oxidation Rate on Vapor Wall Deposition and SOA Mass Yields: A Case Study with α-Pinene Ozonolysis. *Atmos. Chem. Phys.* **2016**, *16*, 9361−9379.
(29) DeRieux, W.-S. W.; Li, Y.; Lin, P.; Laskin, J.; Laskin, A.; Bertram, A. K.; Nizkorodov, S. A.; Shiraiwa, M. Predicting the Glass Transition Temperature and Viscosity of Secondary Organic Material Using Molecular Composition. *Atmos. Chem. Phys.* **2018**, *18*, 6331−6351.
(30) Boyd, C. M.; Sanchez, J.; Xu, L.; Eugene, A. J.; Nah, T.; Tuet, W. Y.; Guzman, M. I.; Ng, N. L. Secondary Organic Aerosol Formation from the β-pinene+NO_3 System: Effect of Humidity and Peroxy Radical Fate. *Atmos. Chem. Phys.* **2015**, *15*, 7497−7522.
(31) Cappa, C. D.; Wilson, K. R. Multi-Generation Gas-Phase Oxidation, Equilibrium Partitioning, and the Formation and Evolution of Secondary Organic Aerosol. *Atmos. Chem. Phys.* **2012**, *12*, 9505−9528.
(32) Jathar, S. H.; Cappa, C. D.; Wexler, A. S.; Seinfeld, J. H.; Kleeman, M. J. Multi-Generational Oxidation Model to Simulate Secondary Organic Aerosol in a 3-D Air Quality Model. *Geosci. Model Dev.* **2015**, *8*, 2553−2567.
(33) Adams, P. J.; Seinfeld, J. H. Predicting Global Aerosol Size Distributions in General Circulation Models. *J. Geophys. Res.* **2002**, *107*, 4370.
(34) Pierce, J. R.; Chen, K.; Adams, P. J. Contribution of Primary Carbonaceous Aerosol to Cloud Condensation Nuclei: Processes and Uncertainties Evaluated with a Global Aerosol Microphysics Model. *Atmos. Chem. Phys.* **2007**, *7*, 5447−5466.
(35) He, Y.; King, B.; Pothier, M.; Lewane, L.; Akherati, A.; Mattila, J.; Farmer, D. K.; McCormick, R. L.; Thornton, M.; Pierce, J. R.; Volckens, J.; Jathar, S. H. Secondary Organic Aerosol Formation from Evaporated Biofuels: Comparison to Gasoline and Correction for Vapor Wall Losses. *Environ. Sci. Process. Impacts* **2020**, *22*, 1461−1474.
(36) Akherati, A.; He, Y.; Coggon, M. M.; Koss, A. R.; Hodshire, A. L.; Sekimoto, K.; Warneke, C.; de Gouw, J.; Yee, L.; Seinfeld, J. H.;

https://dx.doi.org/10.1021/acs.est.0c05796
Environ. Sci. Technol. XXXX, XXX, XXX−XXX

Onasch, T. B.; Herndon, S. C.; Knighton, W. B.; Cappa, C. D.; Kleeman, M. J.; Lim, C. Y.; Kroll, J. H.; Pierce, J. R.; Jathar, S. H. Oxygenated Aromatic Compounds Are Important Precursors of Secondary Organic Aerosol in Biomass-Burning Emissions. *Environ. Sci. Technol.* **2020**, *54*, 8568−8579.
(37) Bianchi, F.; Kurtén, T.; Riva, M.; Mohr, C.; Rissanen, M. P.; Roldin, P.; Berndt, T.; Crounse, J. D.; Wennberg, P. O.; Mentel, T. F.; Wildt, J.; Junninen, H.; Jokinen, T.; Kulmala, M.; Worsnop, D. R.; Thornton, J. A.; Donahue, N.; Kjaergaard, H. G.; Ehn, M. Highly Oxygenated Organic Molecules (HOM) from Gas-Phase Autoxidation Involving Peroxy Radicals: A Key Contributor to Atmospheric Aerosol. *Chem. Rev.* **2019**, *119*, 3472−3509.
(38) Ehn, M.; Thornton, J. A.; Kleist, E.; Sipilä, M.; Junninen, H.; Pullinen, I.; Springer, M.; Rubach, F.; Tillmann, R.; Lee, B.; Lopez-Hilfiker, F.; Andres, S.; Acir, I.-H.; Rissanen, M.; Jokinen, T.; Schobesberger, S.; Kangasluoma, J.; Kontkanen, J.; Nieminen, T.; Kurtén, T.; Nielsen, L. B.; Jørgensen, S.; Kjaergaard, H. G.; Canagaratna, M.; Maso, M. D.; Berndt, T.; Petäjä, T.; Wahner, A.; Kerminen, V.-M.; Kulmala, M.; Worsnop, D. R.; Wildt, J.; Mentel, T. F. A Large Source of Low-Volatility Secondary Organic Aerosol. *Nature* **2014**, *506*, 476−479.
(39) Jokinen, T.; Berndt, T.; Makkonen, R.; Kerminen, V.-M.; Junninen, H.; Paasonen, P.; Stratmann, F.; Herrmann, H.; Guenther, A. B.; Worsnop, D. R.; Kulmala, M.; Ehn, M.; Sipilä, M. Production of Extremely Low Volatile Organic Compounds from Biogenic Emissions: Measured Yields and Atmospheric Implications. *Proc. Natl. Acad. Sci. U.S.A.* **2015**, *112*, 7123−7128.
(40) Kirkby, J.; Duplissy, J.; Sengupta, K.; Frege, C.; Gordon, H.; Williamson, C.; Heinritzi, M.; Simon, M.; Yan, C.; Almeida, J.; Tröstl, J.; Nieminen, T.; Ortega, I. K.; Wagner, R.; Adamov, A.; Amorim, A.; Bernhammer, A.-K.; Bianchi, F.; Breitenlechner, M.; Brilke, S.; Chen, X.; Craven, J.; Dias, A.; Ehrhart, S.; Flagan, R. C.; Franchin, A.; Fuchs, C.; Guida, R.; Hakala, J.; Hoyle, C. R.; Jokinen, T.; Junninen, H.; Kangasluoma, J.; Kim, J.; Krapf, M.; Kürten, A.; Laaksonen, A.; Lehtipalo, K.; Makhmutov, V.; Mathot, S.; Molteni, U.; Onnela, A.; Peräkylä, O.; Piel, F.; Petäjä, T.; Praplan, A. P.; Pringle, K.; Rap, A.; Richards, N. A. D.; Riipinen, I.; Rissanen, M. P.; Rondo, L.; Sarnela, N.; Schobesberger, S.; Scott, C. E.; Seinfeld, J. H.; Sipilä, M.; Steiner, G.; Stozhkov, Y.; Stratmann, F.; Tomé, A.; Virtanen, A.; Vogel, A. L.; Wagner, A. C.; Wagner, P. E.; Weingartner, E.; Wimmer, D.; Winkler, P. M.; Ye, P.; Zhang, X.; Hansel, A.; Dommen, J.; Donahue, N. M.; Worsnop, D. R.; Baltensperger, U.; Kulmala, M.; Carslaw, K. S.; Curtius, J. Ion-Induced Nucleation of Pure Biogenic Particles. *Nature* **2016**, *533*, 521−526.
(41) Shiraiwa, M.; Li, Y.; Tsimpidi, A. P.; Karydis, V. A.; Berkemeier, T.; Pandis, S. N.; Lelieveld, J.; Koop, T.; Pöschl, U. Global Distribution of Particle Phase State in Atmospheric Secondary Organic Aerosols. *Nat. Commun.* **2017**, *8*, No. 15002.
(42) Li, Y.; Shiraiwa, M. Timescales of Secondary Organic Aerosols to Reach Equilibrium at Various Temperatures and Relative Humidities. *Atmos. Chem. Phys.* **2019**, *19*, 5959−5971.
(43) Song, M.; Maclean, A. M.; Huang, Y.; Smith, N. R.; Blair, S. L.; Laskin, J.; Laskin, A.; DeRieux, W.-S. W.; Li, Y.; Shiraiwa, M.; Nizkorodov, S. A.; Bertram, A. K. Liquid−liquid Phase Separation and Viscosity within Secondary Organic Aerosol Generated from Diesel Fuel Vapors. *Atmos. Chem. Phys.* **2019**, *19*, 12515−12529.
(44) Angell, C. A. Formation of Glasses from Liquids and Biopolymers. *Science* **1995**, *267*, 1924−1935.
(45) Evoy, E.; Maclean, A. M.; Rovelli, G.; Li, Y.; Tsimpidi, A. P.; Karydis, V. A.; Kamal, S.; Lelieveld, J.; Shiraiwa, M.; Reid, J. P.; Bertram, A. K. Predictions of Diffusion Rates of Large Organic Molecules in Secondary Organic Aerosols Using the Stokes−Einstein and Fractional Stokes−Einstein Relations. *Atmos. Chem. Phys.* **2019**, *19*, 10073−10085.
(46) D'Ambro, E. L.; Schobesberger, S.; Zaveri, R. A.; Shilling, J. E.; Lee, B. H.; Lopez-Hilfiker, F. D.; Mohr, C.; Thornton, J. A. Isothermal Evaporation of α-Pinene Ozonolysis SOA: Volatility, Phase State, and Oligomeric Composition. *ACS Earth Space Chem.* **2018**, *2*, 1058−1067.
(47) Sato, K.; Fujitani, Y.; Inomata, S.; Morino, Y.; Tanabe, K.; Hikida, T.; Shimono, A.; Takami, A.; Fushimi, A.; Kondo, Y.; Imamura, T.; Tanimoto, H.; Sugata, S. A Study of Volatility by Composition, Heating, and Dilution Measurements of Secondary Organic Aerosol from 1,3,5-Trimethylbenzene. *Atmos. Chem. Phys.* **2019**, *19*, 14901−14915.
(48) Trump, E. R.; Donahue, N. M. Oligomer Formation within Secondary Organic Aerosols: Equilibrium and Dynamic Considerations. *Atmos. Chem. Phys.* **2014**, *14*, 3691−3701.
(49) Pandis, S. N.; Seinfeld, J. H. *Atmospheric Chemistry and Physics: From Air Pollution to Climate Change*; Wiley, 2006.
(50) Riipinen, I.; Pierce, J. R.; Donahue, N. M.; Pandis, S. N. Equilibration Time Scales of Organic Aerosol inside Thermodenuders: Evaporation Kinetics versus Thermodynamics. *Atmos. Environ.* **2010**, *44*, 597−607.
(51) Zhang, X.; Pandis, S. N.; Seinfeld, J. H. Diffusion-Limited Versus Quasi-Equilibrium Aerosol Growth. *Aerosol Sci. Technol.* **2012**, *46*, 874−885.
(52) Shiraiwa, M.; Yee, L. D.; Schilling, K. A.; Loza, C. L.; Craven, J. S.; Zuend, A.; Ziemann, P. J.; Seinfeld, J. H. Size Distribution Dynamics Reveal Particle-Phase Chemistry in Organic Aerosol Formation. *Proc. Natl. Acad. Sci. U.S.A.* **2013**, *110*, 11746−11750.
(53) Koop, T.; Bookhold, J.; Shiraiwa, M.; Pöschl, U. Glass Transition and Phase State of Organic Compounds: Dependency on Molecular Properties and Implications for Secondary Organic Aerosols in the Atmosphere. *Phys. Chem. Chem. Phys.* **2011**, *13*, 19238−19255.
(54) Ziemann, P. J.; Atkinson, R. Kinetics, Products, and Mechanisms of Secondary Organic Aerosol Formation. *Chem. Soc. Rev.* **2012**, *41*, 6582−6605.
(55) Roldin, P.; Eriksson, A. C.; Nordin, E. Z.; Hermansson, E.; Mogensen, D.; Rusanen, A.; Boy, M.; Swietlicki, E.; Svenningsson, B.; Zelenyuk, A.; Pagels, J. Modelling Non-Equilibrium Secondary Organic Aerosol Formation and Evaporation with the Aerosol Dynamics, Gas- and Particle-Phase Chemistry Kinetic Multilayer Model ADCHAM. *Atmos. Chem. Phys.* **2014**, *14*, 7953−7993.
(56) Bakker-Arkema, J. G.; Ziemann, P. J. Measurements of Kinetics and Equilibria for the Condensed Phase Reactions of Hydroperoxides with Carbonyls to Form Peroxyhemiacetals. *ACS Earth Space Chem.* **2020**, *4*, 467−475.
(57) O'Meara, S.; Topping, D. O.; McFiggans, G. The Rate of Equilibration of Viscous Aerosol Particles. *Atmos. Chem. Phys.* **2016**, *16*, 5299−5313.
(58) Price, H. C.; Mattsson, J.; Zhang, Y.; Bertram, A. K.; Davies, J. F.; Grayson, J. W.; Martin, S. T.; O'Sullivan, D.; Reid, J. P.; Rickards, A. M. J.; Murray, B. J. Water Diffusion in Atmospherically Relevant α-Pinene Secondary Organic Material. *Chem. Sci.* **2015**, *6*, 4876−4883.
(59) Song, M.; Liu, P. F.; Hanna, S. J.; Li, Y. J.; Martin, S. T.; Bertram, A. K. Relative Humidity-Dependent Viscosities of Isoprene-Derived Secondary Organic Material and Atmospheric Implications for Isoprene-Dominant Forests. *Atmos. Chem. Phys.* **2015**, *15*, 5145−5159.
(60) Grieshop, A. P.; Donahue, N. M.; Robinson, A. L. Is the Gas-Particle Partitioning in Alpha-Pinene Secondary Organic Aerosol Reversible? *Geophys. Res. Lett.* **2007**, *34*, 305.
(61) Tikkanen, O.-P.; Hämäläinen, V.; Rovelli, G.; Lipponen, A.; Shiraiwa, M.; Reid, J. P.; Lehtinen, K. E. J.; Yli-Juuti, T. Optimization of Process Models for Determining Volatility Distribution and Viscosity of Organic Aerosols from Isothermal Particle Evaporation Data. *Atmos. Chem. Phys.* **2019**, *19*, 9333−9350.
(62) Mu, Q.; Shiraiwa, M.; Octaviani, M.; Ma, N.; Ding, A.; Su, H.; Lammel, G.; Pöschl, U.; Cheng, Y. Temperature Effect on Phase State and Reactivity Controls Atmospheric Multiphase Chemistry and Transport of PAHs. *Sci. Adv.* **2018**, *4*, No. eaap7314.
(63) Cheng, Y.; Su, H.; Koop, T.; Mikhailov, E.; Pöschl, U. Size Dependence of Phase Transitions in Aerosol Nanoparticles. *Nat. Commun.* **2015**, *6*, No. 5923.

https://dx.doi.org/10.1021/acs.est.0c05796
Environ. Sci. Technol. XXXX, XXX, XXX−XXX

(64) Petters, M.; Kasparoglu, S. Predicting the Influence of Particle Size on the Glass Transition Temperature and Viscosity of Secondary Organic Material. *Sci. Rep.* **2020**, *10*, No. 15170.

https://dx.doi.org/10.1021/acs.est.0c05796
Environ. Sci. Technol. XXXX, XXX, XXX−XXX